Thamar University Journal of Natural & Applied Sciences ***8****(2) (2023) 47 – 53*

DOI: https://doi.org/10.59167/tujnas.v8i2.1719

TUJNAS

Original Article

Two-dimensional Materials AlSI, AlSeBr, AlSeI, ScSI, ScSeBr, ScSeCl, ScSeI and InSI for Photocatalytic Water Splitting under Visible Light

Abdulrahman Alhaidar[1,2]

[1] Centre for Materials Science, Queensland University of Technology, Brisbane, QLD 4000, Australia
[2] School of Chemistry and Physics, Science and Engineering Faculty, Queensland University of Technology, Gardens Point Campus, Brisbane, QLD 4000, Australia

Corresponding author: Abdulrahman Alhaidar
Email: e.alhaidar@gmail.com

Received: 16 November 2023. Revised (in revised form): 8 December 2023. Accepted: 9 December 2023. Published: 31 December 2023

Abstract:

This article aims to investigate possible 2D photocatalysts for water splitting and to provide a comprehensive overview of some selected candidate materials from the Computational 2D Materials Database (C2DB). In this article, several 2D materials that have not yet been synthesized or investigated are reviewed. The structure, electronic and optical properties were investigated for many materials, taking into account some criteria for the selection of candidates, such as ABC materials from groups 6 and 7, a band gap of 1.6 to 2.8 eV by HSE calculation, and that these monolayers should be non-magnetic. In this article, it was found that AlSI, AlSeBr, AlSeI, ScSI, ScSeBr, ScSeCl, ScSeI, and InSI (the space groups of these materials are Pmmn (No. 59)) can be used for photocatalytic water splitting. These materials were dynamically stable and possessed excellent visible light absorption. The calculated band gaps were between 2.2 and 2.8 eV and their edge positions of CBM and VBM perfectly matched the oxidation and reduction potentials of water.

Keywords: 2D Materials; Photocatalysis; Water Splitting; Electronic Properties; Optical Properties

1. Introduction

Due to the growing demand for clean and renewable energy, photocatalytic water splitting has attracted intense research interest [1,2]. Photoactive semiconductive photocatalysts play a key role in sunlight-driven water splitting by generating photoexcited electron-hole pairs with redox properties upon light irradiation [3–5]. Traditional three-dimensional (3D) photocatalysts have a low specific surface area, which results in a limited number of reactive sites involved in the water redox reaction. For the interior photoexcited carriers to recombine, they must migrate to the surface. The photocatalytic efficiency of 3D photocatalysts can be limited by such intrinsic flaws [6,7]. Due to their inherent high specific surface areas and low carrier migration distances, 2D photocatalysts have been receiving a great deal of attention in the past decade [8–13].

Utilizing sunlight exposure and photocatalysts, water splitting into (H_2) and (O_2) stands out as a viable technique for converting solar energy into chemical energy. The effectiveness of these photocatalysts is intricately linked to the width of the semiconductor bandgap. Given the inherent advantages of 2D materials, there has been an increasing interest in the potential applications of such materials in the context of photocatalytic water splitting [8,14]. By analyzing the light absorption coefficient and energy band of 2D materials, it becomes possible to explore promising candidates for photocatalysts in water splitting.

Despite the wealth of theoretical and computational studies conducted on various photocatalytic materials, along with proposed strategies to enhance hydrogen evolution efficiency, there remains a critical need for researching novel 2D materials in the realm of photocatalytic water splitting for efficient H_2 fuel production. Furthermore, there has been a recent surge in interest surrounding multi-component metal-oxyhalides in many applications such as photocatalysis and electrocatalysis. Although research into 2D metal oxyhalides is still relatively new compared to other 2D materials like graphene or transition metal dichalcogenides. However, their potential for diverse applications, including photocatalysis, is driving significant attention and investigation in the scientific community.

Several 2D MXY (M= metal; X= O, S, Se, Te; Y= Br, Cl, F, and I) have been recently studied for their unique properties. Others proved the efficacy of lithium oxyhalides, and bismuth oxyhalides in electrocatalysis [15], and photocatalysis [16]. BiOX monolayers (X= Br, Cl and I) have been proven to be potential photocatalysts for water splitting [17]. GaOI and InOI are predicted to have suitable band gaps and band edge for photocatalytic water splitting [18].

A photocatalyst must satisfy several criteria to split water effectively. To split water under sunlight, photoexcited electron-hole pairs must be generated with redox capabilities irradiation [3–5, 9]. Photocatalysts must have band edge positions above and below water's

redox potentials to efficiently utilize solar energy. It is necessary to have a band gap greater than 1.238 eV but less than 3.0 eV to harvest solar energy efficiently [10,19–27]. Photogenerated carriers must also be separated as efficiently as possible to prevent the recombination of surface charges. Additionally, the band edge alignment of the photocatalyst must be suitable. Therefore, the conduction band minimum (CBM) should exceed the reduction potential of H+ / H_2, and the valence band maximum (VBM) should be lower than the oxidation potential of O_2/H_2O (−5.67 eV) [21,22, 24, 28–35]. There are a limited number of qualified photocatalysts that can produce hydrogen because of such stringent requirements.

This article focuses on providing a comprehensive study of materials selected from the Computational 2D Materials Database (C2DB). This database is well-curated and stands out as an exceptional resource for material researchers seeking to explore and select suitable materials for certain applications. It provides detailed computational and structural information, allowing researchers to efficiently screen and evaluate potential candidates for various applications. C2DB contains a large number of materials that might be suitable for water splitting. Since it might be infeasible and time-consuming to study all these materials, are limited for this study to a small subset of photocatalysts by considering some criteria for candidate selection. First, inspired by previous studies on metal-oxyhalides, ABC materials from groups 6 and 7 were selected. The band gaps are from 1.6 to 3.0 eV via HSE calculation, and these monolayers should not be magnetic. Then, conducted a computational study to confirm the reliability of the selected materials for water splitting. Therefore, this study aims to offer an early guideline for further experimental studies on the investigated materials. This article shows that AlSI, AlSeBr, AlSeI, ScSI, ScSeBr, ScSeCl, ScSeI and InSI monolayers possess band gaps from 2.2 and 2.8 eV. In addition, these monolayers have pronounced absorption in the visible light region of the solar spectrum. Their suitable band edge positions and light absorption make them promising photocatalysts.

2. Computational Details

All the calculations were based on Density Functional Theory [36–38] as implemented in the Vienna Ab initio Simulation Package [39–41]. Generalized Gradient Approximation (GGA) of the Perdew-Burke-Ernzerhof (PBE) function was utilized to describe the exchange-correlation function [42,43]. Long-range van der Waals (vdW) interaction was considered based on Grimme scheme s[44]. The gamma-centered k-points grids of 6×8×1 was used for AlSI, AlSeBr, AlSeI, ScSI, ScSeBr, ScSeCl, ScSeI and InSI, and the plane-wave energy cut-off was set to be 500 eV [45]. Atomic positions and cell shapes were fully relaxed until the maximum force acting on atoms and the energy converged to 0.005 eV/Å and 10-6 eV, respectively. A vacuum slab of a minimum of 18 Å was introduced to avoid interaction between neighboring images.

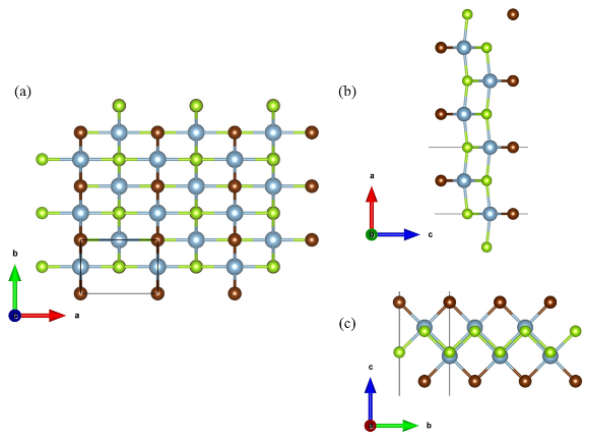

Figure 1: (a) top view and (b and c) sides view of the structure of AlSI, AlSeBr, AlSeI, ScSI, ScSeBr, ScSeCl, ScSeI and InSI monolayers.

The PBE functional method was used to calculate the band gap for these materials to determine if they could be used for water splitting. This calculation was very fast, and the band gap could be seen as a result. To save time, the calculation was stopped if the band gap was higher than 3.0 eV. The PBE functional can underestimate the calculation of band gaps of materials [46], so more accurate results were calculated based on the Heyd-Scuseria-Ernzerhof (HSE06) hybrid functional [47,48]. One important condition to assess the photocatalyst properties of 2D semiconductors is sunlight absorption, and this article used the density functional perturbation (DFPT) method. The spectrum in the visible light region is from 350 to 800 nm. The Phonon calculation was performed by PHONOPY code based on the finite-displacement method [49,50] with the convergence criteria for force and energy at 0.001 eV/Å and 10-8 eV, respectively. Moreover, ab into molecular dynamics simulations was carried out to study the thermal the selected monolayers, performed with a 3×3×1 supercell at 300 K. The simulations lasted for a duration of 10 ps in the NVT ensemble controlled by a Nose–Hoover thermostat [8], [51]. The standard oxidation and reduction potentials, namely, O_2/H_2O = $-5.67\ eV$ and H^+/H_2 = $-4.44\ eV$, were employed.

3. Results and Discussion

3.1 Geometry structure

Optimizing the structure of 2D materials is crucial because their properties are highly sensitive to their atomic arrangement. By tuning the arrangement of atoms, it can enhance specific properties like electronic conductivity, mechanical strength, and optical behavior, making them suitable for various applications in electronics, optics, energy storage, and more. After selecting the materials from the 2D database and the criteria that it has mentioned in the introduction, the zyx file was downloaded and opened via Materials Studio for checking and setup the correct lattice parameter and space group. Then the optimized structure for these monolayers, so can checked if the structures have changed during this calculation. The optimized monolayers for AlSI, AlSeBr, AlSeI, ScSI, ScSeBr, ScSeCl, ScSeI and InSI monolayers crystals are shown in Figure 1. They have trigonal symmetry [52] and Figure 1 (a) shows the top view and (b and c) shows the sides view of these monolayers.

This article has calculated several ABC materials, and it was found that only eight materials could potentially be used for water splitting. However, some of the materials that are not suitable for water splitting might be useful for other applications, such as solar cells. Table 1 shows the eight materials used and the calculated lattice parameters. As shown in Table 1 the calculated lattice parameters of AlSI, AlSeBr, AlSeI, ScSI, ScSeBr, ScSeCl, ScSeI, and InSI monolayers data from previous theoretical studies are well consistent with these findings [53,54]. As the results in Table 1 indicate, lattice constants calculated for the x-axis (a-axis) are larger than for the y-axis (b-axis). It is interesting to note that with increasing atomic mass, the substitution of X atoms has a greater impact on lattice constants and bonds than Y atoms, but the substitution of Y atoms has a greater effect on buckling distances.

To investigate the thermodynamic stability of AlSI, AlSeBr, AlSeI, ScSI, ScSeBr, ScSeCl, ScSeI, and InSI monolayers, their phonon spectra were calculated within the framework of PHONOP. The phonon dispersion spectra of these monolayers were calculated to investigate their dynamic stability. Phonon spectra represent the vibrational modes of a crystalline material as a function of the wave vector in the Brillouin zone. The dispersion diagram generated after this calculation can be used to determine whether the material is dynamically stable, as no imaginary frequencies are present. As can be seen in Figure 2, there are no imaginary frequencies for the phonon modes in the entire Brillouin zone. This shows that these monolayers are dynamically stable. There are six atoms in a primitive cell, resulting in 18 phonon modes, of which three are acoustic and fifteen are optical. According to the calculations, some monolayers were not stable because they did not match the water splitting devices, as shown in Table 2.

Table 1: Calculated structural parameters of AlSI, AlSeBr, AlSeI, ScSI, ScSeBr, ScSeCl, ScSeI and InSI monolayers.

Lattice Parameters	Materials							
	AlSI	**AlSeI**	**AlSeBr**	**ScSeBr**	**ScSeCl**	**InSI**	**ScSI**	**ScSeI**
a (Å)	4.85	5.31	5.23	5.39	5.38	5.32	5.09	5.37
b (Å)	3.71	3.79	3.61	3.83	3.67	3.99	3.92	3.98

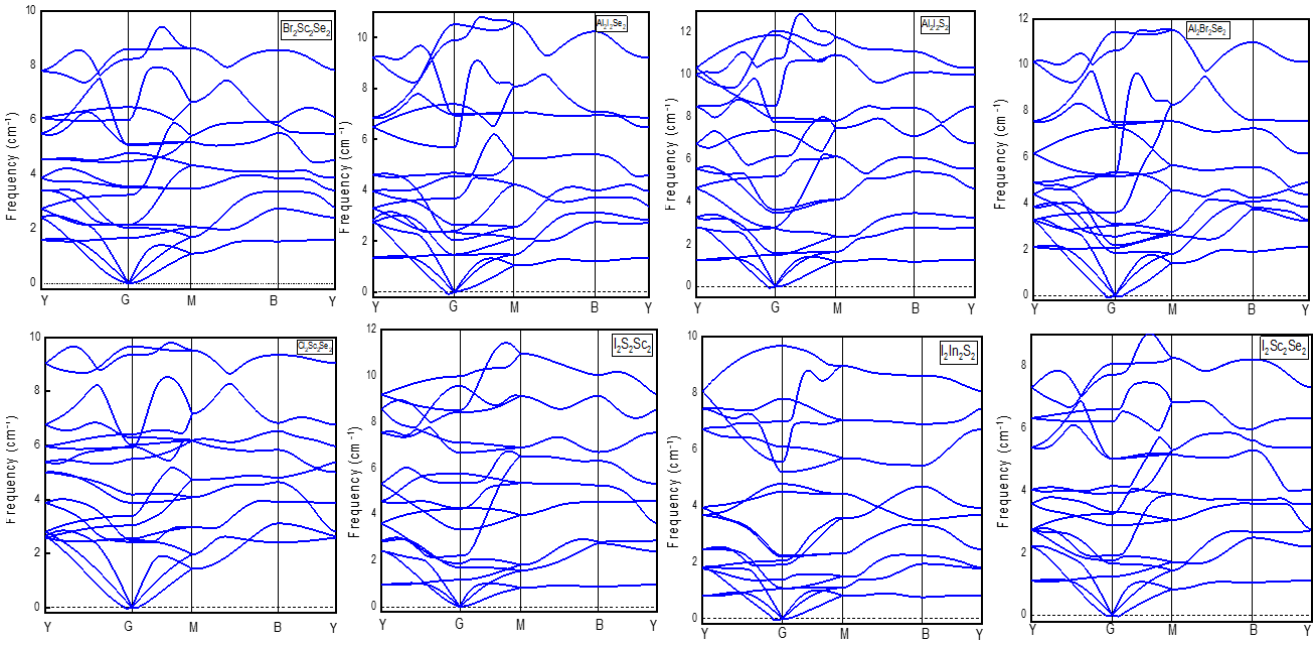

Figure 2: Phonon spectra of AlSI, AlSeBr, AlSeI, ScSI, ScSeBr, ScSeCl, ScSeI, and InSI monolayers with no imaginary frequency in any wave vector.

In addition, AIMD simulations prove thermal stability, for the suitable materials out of the materials that have been selected as the mentioned criteria in the introduction section. Thermal stability typically refers to the ability of a material to maintain its structural and energetic integrity at elevated temperatures. AIMD simulations involve modeling the dynamic behavior of atoms and molecules at finite temperatures and understanding the thermal stability of the system is crucial for various applications including water splitting. The performed colorations for AIMD are set with a 3×3×1 supercell at 300 K and simulation lasting for 10 ps. The time step of 1 fs and NVT ensemble controlled by the Nose-Hoover thermostat [51] was applied in the simulation. As illustrated in Figure 3, the AlSI, AlSeBr, AlSeI, ScSI, ScSeBr, ScSeCl, ScSeI, and InSI monolayers with the energy 300 K and by the time are stable. Moreover, there was no significant structural destruction, and the total energy per atom only fluctuated within a small range (< 0.1 eV) for a period of 10 ps.

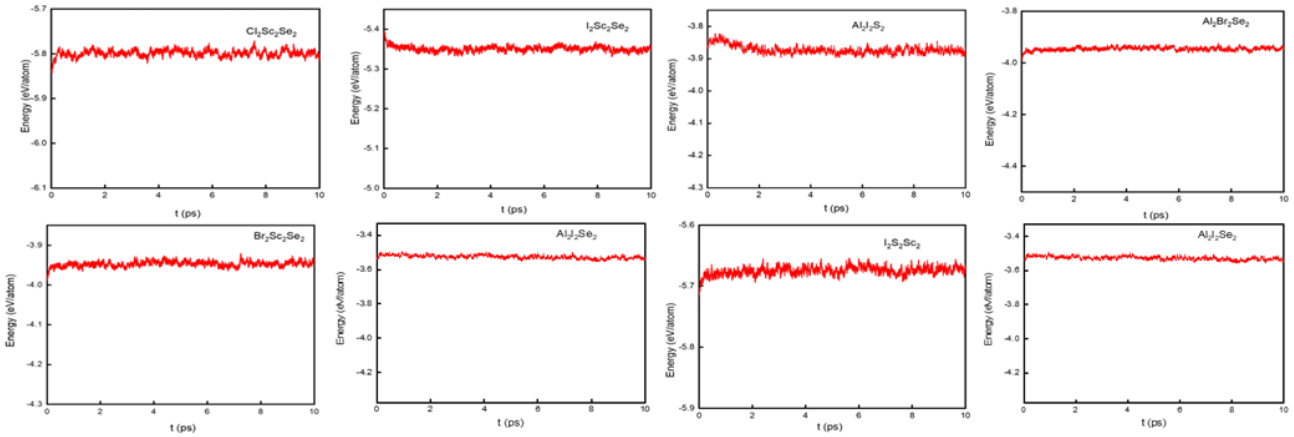

Figure 3: AIMD simulation at 300 K shows the evolution of total energy per atom. The insets are the structures of AlSI, AlSeBr, AlSeI, ScSI, ScSeBr, ScSeCl, ScSeI and InSI monolayers at 0 ps and 10.

3.2 Electronic structures.

The band gap is another important calculation that is composed for water splitting and two methods can get the band gap BPE and HSE06. For accurate results, HSE06 was applied to determine the accurate electronic structure and band gaps of these materials [47,48]. Figure 4 shows the HSE06 functional calculation obtained from indirect band gaps of AlSI, AlSeBr, AlSeI, ScSI, ScSeBr, ScSeCl, ScSeI, and InSI monolayers are 2.56, 2.27, 2.22, 2.8, 2.4, 2.29, 2.38 and 2.49, respectively. By comparing these values with the band gap of Ag2S and NaTAO3 monolayer, which is approximately 2.83 and 2.25 eV, most of the values are quite close to Ag2S and NaTAO3 which have been identified as photocatalysts for water splitting [55], [56]. After that, several materials were investigated (see Table 2), however, some of these materials are not used as photocatalytic water splitters due to large band gaps (over 3 eV).

3.3 Photocatalytic properties.

As described in the introduction, for 2D materials to be used as efficient photocatalysts, they must have suitable band edge positions. That is, the CBM of the photocatalyst should be above the reduction potential of water, -4.44 eV, and the VBM should be lower than the oxidation potential of water, -5.67 eV [21,28,57]. The VBMs are calculated from the difference between the vacuum potential and Fermi level. As shown in Figure 5, the CBMs of the monolayers were above -4.44 eV, which is greater than the hydrogen reduction potential. The VBMs of these monolayers were not below the water oxidation potential, -5.67 eV. The band edge positions are connected to the water redox potentials, which means that these monolayers could work as photocatalysts without an external bias voltage [8,58,59]. The calculated positions of VBM and CBM are shown in a schematic diagram in Figure 5 the red line indicates the CBM level, and the blue line indicates the VBM level. The VBM band edges of these monolayers were located at approximately -7.1 eV, which is significantly lower than the oxidation potential of water, whereas the CBM of the monolayers was slightly higher than the reduction potential of water. Therefore, the AlSI, AlSeBr, AlSeI, ScSI, ScSeBr, ScSeCl, ScSeI, and InSI monolayers are suitable for water splitting after approval via this calculation. There are some monolayers that are laminated after checking the band position because the CBM or VBM does not fit with the requirement mentioned and shown in Table 2.

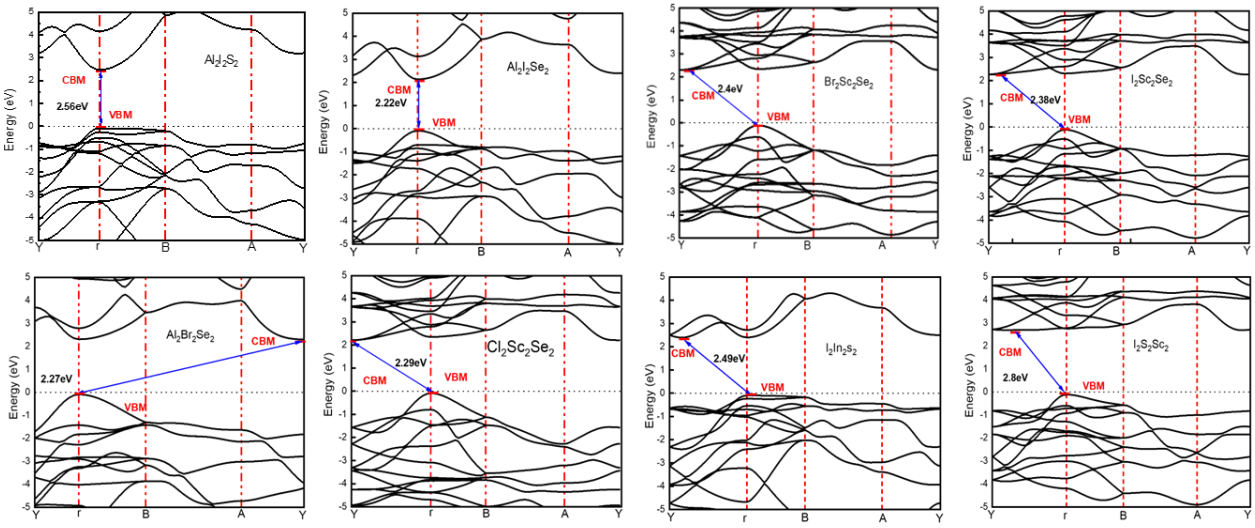

Figure 4: The band structures on the HSE06 level of the AlSI, AlSeBr, AlSeI, ScSI, ScSeBr, ScSeCl, ScSeI, and InSI monolayers and the range are between 2.2 to 2.8 eV.

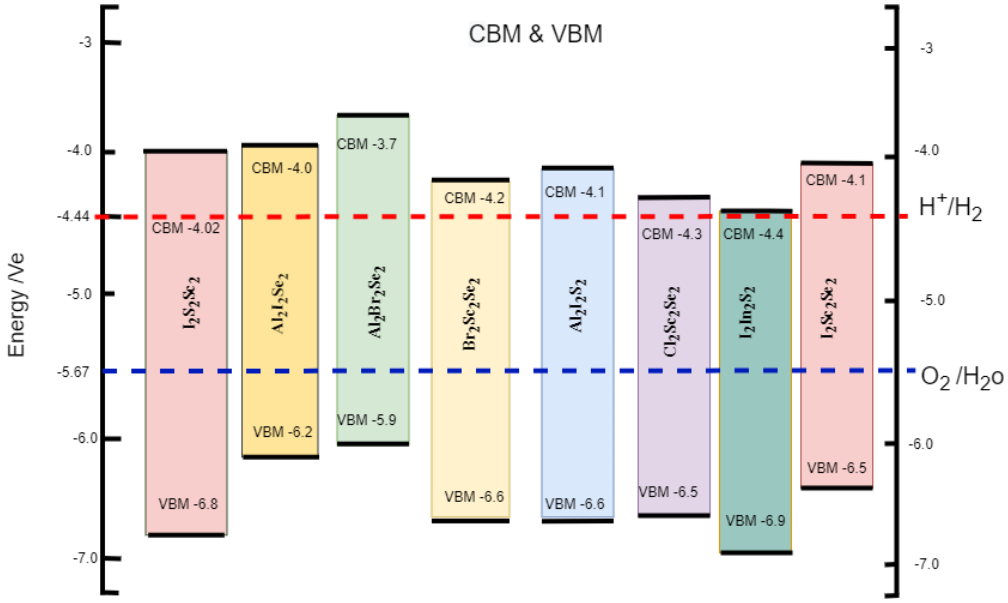

Figure 5: shows the band positions of AlSI, AlSeBr, AlSeI, ScSI, ScSeBr, ScSeCl, ScSeI, and InSI monolayers compared to the redox potential of water splitting.

Table 2: the selected materials from the 2D database (D2CB).

Materials	HSE band gap	eV	CBM	VBM
BrInS	2.8046	3.469	-4.445	-7.249
AsClTe	1.5756	3.097	-4.533	-6.109
BrGaS	2.3418	3.25	-4.677	-7.02
BrSSc	3.2455	3.162	-4.149	-7.394
ClGaS	2.3179	3.276	-4.646	-6.966
ClHfN	3.325	3.295	-3.534	-6.86
ClInO	4.1147	3.789	-4.563	-8.677
ClInS	2.7986	3.531	-4.489	-7.288
ClSSc	3.1288	3.153	-4.204	-7.333
ClScSe	2.2973	2.966	-4.257	-6.554
AsClSe	2.26	3.328	-4.937	-7.197
BrSbSe	1.8102	3.823	-5.139	-6.948
AlBrS	3.1703	3.466	-3.57	-6.74
AlClS	3.2446	3.5	-3.2	-6.45
AlClSe	2.1058	3.231	-3.53	-5.64
AlIS	2.5641	4.05	-4.08	-6.64
AlISe	2.2269	3.731	-3.96	-6.19
BrGaO	4.0447	3.475	-3.5	-7.55
BrHfN	3.279	3.325	-3.572	-6.851
BrInO	3.6043	3.769	-4.385	-7.990
BrNZr	3.7087	4.328	-3.027	-6.728
AlBrSe	2.2725	3.205	-3.682	-5.954
AsClTe	1.5756	3.097	-4.533	-6.109
HfIN	2.7113	4.03	-3.637	-6.168
IInS	2.49	3.93	-4.41	-6.901
ISSc	2.8	3.701	-4.026	-6.827
IScSe	2.381	3.52	-4.106	-6.488
AsClSe	2.26	3.328	-4.937	-7.20
BrSbSe	1.8102	3.823	-5.139	-6.948

3.4 Optical absorption.

Another important property to assess for a photocatalyst is its ability to absorb sunlight. High response to a broad range of solar light is highly desirable for generating more electron-hole pairs for the full utilization of solar energy. Using the dielectric function with the HSE06 hybrid functional, the absorption coefficient was calculated from the complex dielectric constants and Energy conversion can be more efficient when there is a high response to solar light. A spectrum of visible light (approximately 350 - 800 nm). Figure 6 shows that light absorption occurs predominantly in the ultraviolet (UV) range, with a small contribution from the visible range. These monolayers have significant absorption peaks in the ultraviolet range, as well as in the x- and y-directions. Usually, solar blind deep-UV detectors operate under severe conditions, which allows these monolayers to be used in UV optoelectronic devices in solar blinds. Moreover, the light absorption of AlSI, AlSeBr, AlSeI, ScSI, ScSeBr, ScSeCl, ScSeI, and InSI monolayers were 500, 420, 430, 550, 420, 510, 510, and 440 nm, as shown in Figure 6. These materials exhibit highly favorable phonon spectra that closely resemble those of synthesized and experimentally investigated materials such as the CdS nanorod/ZnS nanoparticle composite [60]. It is worth mentioning that there are some of the materials having large band gaps (over 3 eV) which indicate that large band gaps can have poor light absorption, as can be seen in Table 2.

4. Conclusion

In this article, the electronic structure, band edge positions, phonon spectra, and light absorption were calculated for a wide range of unsynthesized materials. After calculating their phonon spectra, it is found that there is no imaginary frequency in the monolayers AlSI, AlSeBr, AlSeI, ScSI, ScSeBr, ScSeCl, ScSeI, and InSI. This finding indicates that some of these monolayers are dynamically stable, while for the remaining monolayers, which have a small imaginary frequency, the problem could be solved by enlarging the supercell. Furthermore, the light absorption was calculated, and these monolayers have good light absorption at around 420 and 680 nm. Moreover, the band gaps of the AlSI, AlSeBr, AlSeI, ScSI, ScSeBr, ScSeCl, ScSeI, and InSI monolayers are between 2.2 and 2.8 eV, which is an excellent position for water splitting. The CBMs and the VBMs have exceptional suitability for the oxidation and reduction potentials of water. According to our findings, these materials have an excellent band gap position, and some of these monolayers are dynamically stable and have good light absorption. These 2D materials are suitable photocatalysts for photoelectrochemical water splitting. Therefore, they could be promising photocatalysts for water splitting. Our work not only enriches the family of 2D materials but also reveals new candidates for the development of highly efficient photocatalysts soon.

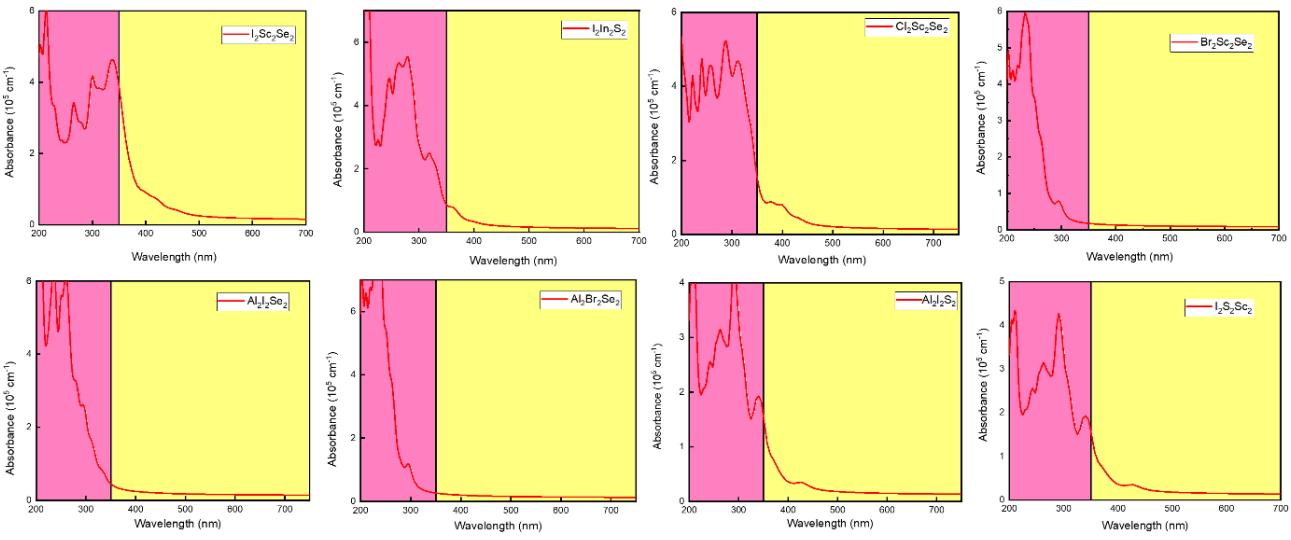

Figure 6: Calculated light absorption of these monolayers in direction. Purple and yellow areas represent the ultraviolet and visible regions of sunlight.

References

[1] Fujishima, A., Honda, K. (1972) Electrochemical photolysis of water at a semiconductor electrode, *Nature* **238**: 37-38.

[2] Grätzel, M. (2001) Photoelectrochemical cells, *Nature* **414**: 338-344.

[3] McCrory, C.C., Jung, S., Ferrer, I.M., Chatman, S.M., Peters, J.C., Jaramillo, T.F. (2015) Benchmarking hydrogen evolving reaction and oxygen evolving reaction electrocatalysts for solar water splitting devices, *Journal of the American Chemical Society* **137**: 4347-4357.

[4] Chen, X., Shen, S., Guo, L., Mao, S.S. (2010) Semiconductor-based photocatalytic hydrogen generation, *Chemical Reviews* **110**: 6503-6570.

[5] Walter, M.G., Warren, E.L., McKone, J.R., Boettcher, S.W., Mi, Q., Santori, E.A., Lewis, N.S. (2010) Solar water splitting cells, *Chemical Reviews* **110**: 6446-6473.

[6] Kudo, A., Miseki, Y. (2009) Heterogeneous photocatalyst materials for water splitting, *Chemical Society Reviews* **38**: 253-278.

[7] Takanabe, K. (2017) Photocatalytic water splitting: quantitative approaches toward photocatalyst by design, *ACS Catalysis* **7**: 8006-8022.

[8] Qiao, M., Liu, J., Wang, Y., Li, Y., Chen, Z. (2018) $PdSeO_3$ monolayer: promising inorganic 2D photocatalyst for direct overall water splitting without using sacrificial reagents and cocatalysts, *Journal of the American Chemical Society* **140**: 12256-12262.

[9] Li, Y., Li, Y.-L., Sa, B., Ahuja, R. (2017) Review of two-dimensional materials for photocatalytic water splitting from a theoretical perspective, *Catalysis Science & Technology* **7**: 545-559.

[10] Zhang, X., Zhao, X., Wu, D., Jing, Y., Zhou, Z. (2016) $MnPSe_3$ monolayer: A promising 2D visible-light photohydrolytic catalyst with high carrier mobility, *Advanced Science* **3**: 1600062.

[11] Zhao, P., Ma, Y., Lv, X., Li, M., Huang, B., Dai, Y. (2018) Two-dimensional III2-VI3 materials: Promising photocatalysts for overall water splitting under infrared light spectrum, *Nano Energy* **51**: 533-538.

[12] Fu, C.-F., Sun, J., Luo, Q., Li, X., Hu, W., Yang, J. (2018) Intrinsic electric fields in two-dimensional materials boost the solar-to-hydrogen efficiency for photocatalytic water splitting, *Nano Letters* **18**: 6312-6317.

[13] Alhaidar, A., Du, A., Zhang, L. (2022) Two-dimensional $MgAl_2S_4$ as potential photocatalyst for water splitting and strategies to boost its performance, *Applied Surface Science* **605**: 154826.

[14] Yao, S., Zhang, X., Zhang, Z., Chen, A., Zhou, Z. (2019) 2D Triphosphides: SbP_3 and GaP_3 monolayer as promising photocatalysts for water splitting, *International Journal of Hydrogen Energy* **44**: 5948-5954.

[15] García de Arquer, F.P., Bushuyev, O.S., De Luna, P., Dinh, C.T., Seifitokaldani, A., Saidaminov, M.I., Tan, C.S., Quan, L.N., Proppe, A., Kibria, M.G. (2018) 2D metal oxyhalide-derived catalysts for efficient CO_2 electroreduction, *Advanced Materials* **30**: 1802858.

[16] Di, J., Xia, J., Li, H., Guo, S., Dai, S. (2017) Bismuth oxyhalide layered materials for energy and environmental applications, *Nano Energy* **41**: 172-192.

[17] Cheng, H., Huang, B., Dai, Y. (2014) Engineering BiOX (X= Cl, Br, I) nanostructures for highly efficient photocatalytic applications, *Nanoscale* **6**: 2009-2026.

[18] He, J., Lyu, P., Nachtigall, P. (2020) Two-dimensional tetragonal GaOI and InOI sheets: In-plane anisotropic optical properties and application to photocatalytic water splitting, *Catalysis Today* **340**: 178-182.

[19] Ji, Y., Yang, M., Dong, H., Hou, T., Wang, L., Li, Y. (2017) Two-dimensional germanium monochalcogenide photocatalyst for water splitting under ultraviolet, visible to near-infrared light, *Nanoscale* **9**: 8608-8615.

[20] Wang, Q., Nakabayashi, M., Hisatomi, T., Sun, S., Akiyama, S., Wang, Z., Pan, Z., Xiao, X., Watanabe, T., Yamada, T. (2019) Oxysulfide photocatalyst for visible-light-driven overall water splitting, *Nature Materials* **18**: 827-832.

[21] Ni, M., Leung, M.K., Leung, D.Y., Sumathy, K. (2007) A review and recent developments in photocatalytic water-splitting using TiO_2 for hydrogen production, *Renewable and Sustainable Energy Reviews* **11**: 401-425.

[22] Cook, T.R., Dogutan, D.K., Reece, S.Y., Surendranath, Y., Teets, T.S., Nocera, D.G. (2010) Solar energy supply and storage for the legacy and nonlegacy worlds, *Chemical Reviews* **110**: 6474-6502.

[23] Zhang, X., Zhang, Z., Wu, D., Zhang, X., Zhao, X., Zhou, Z. (2018) Computational screening of 2D materials and rational design of heterojunctions for water splitting photocatalysts, *Small Methods* **2**: 1700359.

[24] Zhuang, H.L., Hennig, R.G. (2013) Single-layer group-III monochalcogenide photocatalysts for water splitting, *Chemistry of Materials* **25**: 3232-3238.

[25] Chowdhury, C., Karmakar, S., Datta, A. (2017) Monolayer group IV–VI monochalcogenides: low-dimensional materials for photocatalytic water splitting, *The Journal of Physical Chemistry C* **121**: 7615-7624.

[26] Jiang, X., Wang, P., Zhao, J. (2015) 2D covalent triazine framework: a new class of organic photocatalyst for water splitting, *Journal of Materials Chemistry A* **3**: 7750-7758.

[27] Peng, Q., Xiong, R., Sa, B., Zhou, J., Wen, C., Wu, B., Anpo, M., Sun, Z. (2017) Computational mining of photocatalysts for water splitting hydrogen production: two-dimensional InSe-family monolayers, *Catalysis Science & Technology* **7**: 2744-2752.

[28] Khaselev, O., Turner, J.A. (1998) A monolithic photovoltaic-photoelectrochemical device for hydrogen production via water splitting, *Science* **280**: 425-427.

[29] Lin, Y., Yuan, G., Liu, R., Zhou, S., Sheehan, S.W., Wang, D. (2011) Semiconductor nanostructure-based photoelectrochemical water splitting: a brief review, *Chemical Physics Letters* **507**: 209-215.

[30] Su, J., Guo, L., Bao, N., Grimes, C.A. (2011) Nanostructured WO_3/$BiVO_4$ heterojunction films for efficient photoelectrochemical water splitting, *Nano Letters* **11**: 1928-1933.

[31] Singh, A.K., Mathew, K., Zhuang, H.L., Hennig, R.G. (2015) Computational screening of 2D materials for photocatalysis, *The Journal of Physical Chemistry Letters* **6**: 1087-1098.

[32] Hisatomi, T., Kubota, J., Domen, K. (2014) Recent advances in semiconductors for photocatalytic and photoelectrochemical water splitting, *Chemical Society Reviews* **43**: 7520-7535.

[33] Luo, B., Liu, G., Wang, L. (2016) Recent advances in 2D materials for photocatalysis, *Nanoscale* **8**: 6904-6920.

[34] Rahman, M.Z., Kwong, C.W., Davey, K., Qiao, S.Z. (2016) 2D phosphorene as a water splitting photocatalyst: fundamentals to applications, *Energy & Environmental Science* **9**: 709-728.

[35] Yang, L., Li, X., Zhang, G., Cui, P., Wang, X., Jiang, X., Zhao, J., Luo, Y., Jiang, J. (2017) Combining photocatalytic hydrogen generation and capsule storage in graphene based sandwich structures, *Nature Communications* **8**: 16049.

[36] Sham, L.J., Schlüter, M. (1983) Density-functional theory of the energy gap, *Physical Review Letters* **51**: 1888.

[37] Gross, E., Kohn, W. (1985) Local density-functional theory of frequency-dependent linear response, *Physical Review Letters* **55**: 2850.

[38] Kresse, G., Furthmüller, J., Hafner, J. (1995) Ab initio force constant approach to phonon dispersion relations of diamond and graphite, *Europhysics Letters* **32**: 729.

[39] Kresse, G., Hafner, J. (1994) Ab initio molecular-dynamics simulation of the liquid-metal–amorphous-semiconductor transition in germanium, *Physical Review B* **49**: 14251.

[40] Kresse, G., Furthmüller, J. (1996) Efficiency of ab-initio total energy calculations for metals and semiconductors using a plane-wave basis set, *Computational Materials Science* **6**: 15-50.

[41] Kresse, G., Furthmüller, J. (1996) Efficient iterative schemes for ab initio total-energy calculations using a plane-wave basis set, *Physical Review B* **54**: 11169.

[42] Perdew, J.P., Burke, K., Ernzerhof, M. (1996) Generalized gradient approximation made simple, *Physical Review Letters* **77**: 3865.

[43] Grimme, S. (2006) Semiempirical GGA-type density functional constructed with a long-range dispersion correction, *Journal of Computational Chemistry* **27**: 1787-1799.

[44] Perdew, J.P., Ernzerhof, M., Burke, K. (1996) Rationale for mixing exact exchange with density functional approximations, *The Journal of Chemical Physics* **105**: 9982-9985.

[45] Monkhorst, H.J., Pack, J.D. (1976) Special points for Brillouin-zone integrations, *Physical Review B* **13**: 5188.

[46] Krukau, A.V., Vydrov, O.A., Izmaylov, A.F., Scuseria, G.E. (2006) Influence of the exchange screening parameter on the performance of screened hybrid functionals, *The Journal of Chemical Physics* **125**.

[47] Heyd, J., Peralta, J.E., Scuseria, G.E., Martin, R.L. (2005) Energy band gaps and lattice parameters evaluated with the Heyd-Scuseria-Ernzerhof screened hybrid functional, *The Journal of Chemical Physics* **123**.

[48] Heyd, J., Scuseria, G.E., Ernzerhof, M. (2003) Hybrid functionals based on a screened Coulomb potential, *The Journal of Chemical Physics* **118**: 8207-8215.

[49] Togo, A., Tanaka, I. (2015) First principles phonon calculations in materials science, *Scripta Materialia* **108**: 1-5.
[50] Baroni, S., De Gironcoli, S., Dal Corso, A., Giannozzi, P. (2001) Phonons and related crystal properties from density-functional perturbation theory, *Reviews of Modern Physics* **73**: 515.
[51] Martyna, G.J., Klein, M.L., Tuckerman, M. (1992) Nosé–Hoover chains: The canonical ensemble via continuous dynamics, *The Journal of Chemical Physics* **97**: 2635-2643.
[52] Ma, F., Zhou, M., Jiao, Y., Gao, G., Gu, Y., Bilic, A., Chen, Z., Du, A. (2015) Single layer bismuth iodide: computational exploration of structural, electrical, mechanical and optical properties, *Scientific Reports* **5**: 17558.
[53] Qi, H., Sun, Z., Wang, N., Qin, G., Zhang, H., Shen, C. (2021) Two-dimensional $Al_2I_2Se_2$: a promising anisotropic thermoelectric material, *Journal of Alloys and Compounds* **876**: 160191.
[54] Haastrup, S., Strange, M., Pandey, M., Deilmann, T., Schmidt, P.S., Hinsche, N.F., Gjerding, M.N., Torelli, D., Larsen, P.M., Riis-Jensen, A.C. (2018) The Computational 2D Materials Database: high-throughput modeling and discovery of atomically thin crystals, *2D Materials* **5**: 042002.
[55] Peng, R., Ma, Y., He, Z., Huang, B., Kou, L., Dai, Y. (2019) Single-layer Ag_2S: a two-dimensional bidirectional auxetic semiconductor, *Nano Letters* **19**: 1227-1233.
[56] Liu, Y.-L., Yang, C.-L., Wang, M.-S., Ma, X.-G., Yi, Y.-G. (2018) Te-doped perovskite $NaTaO_3$ as a promising photocatalytic material for hydrogen production from water splitting driven by visible light, *Materials Research Bulletin* **107**: 125-131.
[57] Bai, Y., Zhang, Q., Luo, G., Bu, Y., Zhu, L., Fan, L., Wang, B. (2017) $GaS_{0.5}Te_{0.5}$ monolayer as an efficient water splitting photocatalyst, *Physical Chemistry Chemical Physics* **19**: 15394-15402.
[58] Matta, S.K., Zhang, C., Jiao, Y., O'Mullane, A., Du, A. (2018) Versatile two-dimensional silicon diphosphide (SiP_2) for photocatalytic water splitting, *Nanoscale* **10**: 6369-6374.
[59] Ashwin Kishore, M., Ravindran, P. (2017) Tailoring the electronic band gap and band edge positions in the C_2N monolayer by P and as substitution for photocatalytic water splitting, *The Journal of Physical Chemistry C* **121**: 22216-22224.
[60] Jiang, D., Sun, Z., Jia, H., Lu, D., Du, P. (2016) A cocatalyst-free CdS nanorod/ZnS nanoparticle composite for high-performance visible-light-driven hydrogen production from water, *Journal of Materials Chemistry A* **4**: 675-683.